ARTICLE Communicated by Bard Ermentrout

Synchronization in Networks of Excitatory and Inhibitory Neurons with Sparse, Random Connectivity

Christoph Börgers
christoph.borgers@tufts.edu
Department of Mathematics, Tufts University, Medford, MA 02155, U.S.A.

Nancy Kopell
nk@math.bu.edu
Department of Mathematics and Center for BioDynamics, Boston University, Boston, MA 02215, U.S.A.

In model networks of E-cells and I-cells (excitatory and inhibitory neurons, respectively), synchronous rhythmic spiking often comes about from the interplay between the two cell groups: the E-cells synchronize the I-cells and vice versa. Under ideal conditions—homogeneity in relevant network parameters and all-to-all connectivity, for instance—this mechanism can yield perfect synchronization. We find that approximate, imperfect synchronization is possible even with very sparse, random connectivity. The crucial quantity is the expected number of inputs per cell. As long as it is large enough (more precisely, as long as the variance of the total number of synaptic inputs per cell is small enough), tight synchronization is possible. The desynchronizing effect of random connectivity can be reduced by strengthening the E→I synapses. More surprising, it cannot be reduced by strengthening the I→E synapses. However, the decay time constant of inhibition plays an important role. Faster decay yields tighter synchrony. In particular, in models in which the inhibitory synapses are assumed to be instantaneous, the effects of sparse, random connectivity cannot be seen.

1 Introduction

In networks of E-cells (excitatory neurons) and I-cells (inhibitory neurons), synchronous, rhythmic spiking often results from the interplay between the two cell groups, with the E-cells synchronizing the I-cells and vice versa. This mechanism, called PING (pyramidal interneuronal network gamma; Whittington, Traub, Kopell, Ermentrout, & Buhl, 2000) or γ-II (Tiesinga, Fellous, José, & Sejnowski, 2001), has been observed in modeling studies, and there are reasons to believe that some experimentally observed gamma rhythms are in fact based on this mechanism (Traub, Jefferys, & Whittington, 1999; Whittington et al., 2000; Tiesinga et al., 2001).

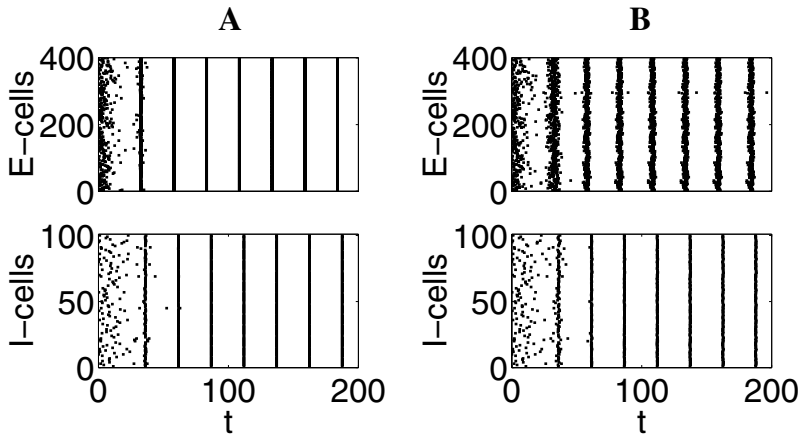

Figure 1: PING in E-I networks with (A) all-to-all connectivity and (B) sparse connectivity.

The conditions under which PING occurs are not completely understood, though we discuss them heuristically in section 6. We focus here on the effects of random connectivity on PING. This effect is illustrated by Figure 1. Details about this figure will be given later. For now, it suffices to say that Figure 1A shows the emergence of PING in a model E/I network with all-to-all connectivity and without any kind of heterogeneity in network parameters. The figure indicates spike times. Both cell groups (E and I) synchronize tightly. If the connectivity is made sparse and random, Figure 1A turns into Figure 1B. The two cell groups now fire spike volleys of brief but positive duration. (The spike volleys of the I-cells are so brief that they appear to have zero duration in the plot.) The main goal of this article is to analyze the durations and shapes of these volleys and their dependence on network parameters.

Synchronization in the presence of random connectivity has been studied previously for excitatory networks (Barkai, Kanter, & Sompolinsky, 1990), inhibitory networks (Brunel & Hakim, 1999; Wang & Buzsáki, 1996), and E/I networks (Brunel, 2000; Bush & Sejnowski, 1996; Golomb & Hansel, 2000; Hansel & Mato, 2001; van Vreeswijk & Sompolinsky, 1996, 1998; Wang, Golomb, & Rinzel, 1995). This literature is aimed at understanding either the stability of the asynchronous state or transitions from asynchrony to rhythms and vice versa. We do not consider these issues here, but focus instead on a detailed understanding of the near-synchronous state.

In section 2, we review the theta model (Ermentrout & Kopell, 1986; Gutkin & Ermentrout, 1998; Hoppensteadt & Izhikevich, 1997), an idealization of a large class of conductance-based neuronal models. Our arguments and simulations in this article are based on this model. We also introduce

our model of synapses in section 2 and describe the connectivity of our model networks. In section 3, we present numerical experiments demonstrating that the desynchronizing effect of sparseness and randomness in the connectivity primarily originates from the variance in the number of inputs per cell, not from the randomness per se. The synchronization of a population of cells by an inhibitory input pulse is analyzed in section 4, first assuming that all cells receive the same input pulse, and then, motivated by the result of section 3, assuming that different cells receive input pulses of different strengths. Similarly, the synchronization of a population of cells by an excitatory input pulse is analyzed in section 5, first assuming that all cells receive the same input pulse, then assuming that different cells receive input pulses of different strengths. The results of sections 4 and 5 are combined in section 6 to analyze PING in E/I networks. In section 7, we summarize our results and put them into the context of other recent work on the same subject.

2 Review of Theta Neurons

2.1 Equation of a Single Theta Neuron. In the Hodgkin-Huxley model, a periodically spiking space-clamped neuron is represented by a point moving on a limit cycle in a four-dimensional phase space. Analogously, in the theta model (Ermentrout & Kopell, 1986; Gutkin & Ermentrout, 1998; Hoppensteadt & Izhikevich, 1997), a neuron is represented by a point $P = (\cos\theta, \sin\theta)$ moving on the unit circle S^1. In the absence of synaptic coupling, the differential equation governing the motion is

$$\frac{d\theta}{dt} = \frac{1}{\tau}(1 - \cos\theta) + I(1 + \cos\theta). \tag{2.1}$$

Here, I should be thought of as an input "current," measured in radians per unit time. The time constant $\tau > 0$ is needed to make equation 2.1 dimensionally correct; it is analogous to a membrane time constant.

When $I < 0$, equation 2.1 has the two fixed points:

$$\theta_0^{\pm} = \pm 2 \arccos \frac{1}{\sqrt{1 - \tau I}}.$$

θ_0^- is stable, and θ_0^+ is unstable. For $I < 0$, the vector field on the circle is shown in the left panel of Figure 2A. If θ is perturbed slightly from θ_0^-, it returns to θ_0^-. However, if θ is raised beyond θ_0^+, a large excursion occurs, with the point P moving around the entire circle while θ increases to $\theta_0^- + 2\pi$. The stable fixed point θ_0^- is the analog of the stable equilibrium of a neuron. The unstable fixed point θ_0^+ is the analog of a spiking threshold.

As I approaches 0, the fixed points approach each other. A saddle-node bifurcation occurs when $I = 0$. The two fixed points come together at $\theta = 0$ (see the center panel of Figure 2A). When $I > 0$, $d\theta/dt > 0$ for all t, so there is no fixed point (see the right panel of Figure 2A).

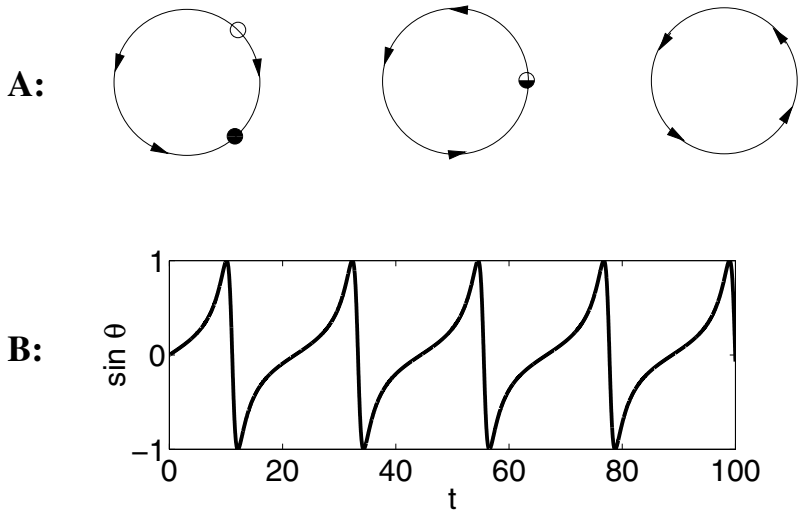

Figure 2: Theta model. (A) Vector field on the circle for $I < 0$, $I = 0$, and $I > 0$. (B) $\sin\theta$ as a function of time.

The transition from $I < 0$ to $I > 0$ is the analog of the transition from excitability to spiking in a neuron. Neuronal models are called of type I if this transition involves a saddle-node bifurcation on a limit cycle and of type II if it involves a subcritical Hopf bifurcation (Ermentrout, 1996; Gutkin & Ermentrout, 1998; Rinzel & Ermentrout, 1998). This classification goes back to Hodgkin (1948). Thus, the theta model is a type I neuronal model. It has been shown to be canonical, in the sense that other type I models can be reduced to it by coordinate transformations (Ermentrout & Kopell, 1986; Hoppensteadt & Izhikevich, 1997).

If $0 < I \ll 1/\tau$, the motion is much slower near $\theta = 0$, that is, near the "ghost" of the fixed point annihilated in the saddle-node bifurcation, than elswhere. This is illustrated in Figure 2B, which shows $\sin\theta$ as a function of t for $\tau = 1, I = 0.02$. As the point $P = (\cos\theta, \sin\theta)$ moves slowly past $(1, 0)$, $\sin\theta$ changes slowly. As P moves rapidly around the circle, $\sin\theta$ rapidly rises to 1, then falls to -1, then returns to values slightly below 0. To some extent the graph of $\sin\theta$ resembles the voltage trace of a spiking neuron.[1]

[1] Some authors think of $-\cos\theta$, not $\sin\theta$, as the "voltage-like" quantity in the theta model. Which of the two we call voltage-like is of no consequence for this article, and neither is voltage-like in any precise sense. However, we prefer to think of $\sin\theta$ as the voltage-like quantity for the following aesthetic reason. Consider a theta neuron driven slightly above threshold. Near the ghost of the equilibrium point ($\theta = 0$), $\sin\theta$ is slowly increasing, while $-\cos\theta$ has a local minimum. On the other hand, for a Hodgkin-Huxley-type neuron of type I driven slightly above threshold, the membrane potential V is slowly

When θ crosses $(2l-1)\pi$, l integer, with $d\theta/dt > 0$, we say that the neuron spikes.

If $I > 0$ and $-\pi \le \theta_1 \le \theta_2 \le \pi$, the time it takes for θ to rise from θ_1 to θ_2 equals

$$\int_{\theta_1}^{\theta_2} \frac{d\theta}{(1-\cos\theta)/\tau + I(1+\cos\theta)} = \sqrt{\frac{\tau}{I}} \left[\arctan \frac{\tan(\theta/2)}{\sqrt{\tau I}} \right]_{\theta_1}^{\theta_2}. \tag{2.2}$$

Setting $\theta_1 = -\pi$ and $\theta_2 = \pi$ in this formula, we find that the period equals

$$P = \pi \sqrt{\frac{\tau}{I}}. \tag{2.3}$$

We denote the time it takes for θ to rise from $\pi/2$ to $3\pi/2$ by W and call it the spike width. Applying formula 2.2 with $(\theta_1, \theta_2) = (\pi/2, \pi)$ and $(\theta_1, \theta_2) = (-\pi, -\pi/2)$ and adding the results, we find

$$W = \left[\pi - 2 \arctan \frac{1}{\sqrt{\tau I}} \right] \sqrt{\frac{\tau}{I}}. \tag{2.4}$$

For physiological realism, we wish to ensure $W/P \ll 1$. By equations 2.3 and 2.4,

$$\frac{W}{P} = 1 - \frac{2}{\pi} \arctan \frac{1}{\sqrt{\tau I}}.$$

Therefore, $W/P \ll 1$ means the same as $\tau I \ll 1$. Since $\arctan(1/\epsilon) = \pi/2 - \epsilon + O(\epsilon^2)$ as $\epsilon \to 0$, equation 2.4 implies $W \approx 2\tau$ when $\tau I \ll 1$. Thus, in the parameter regime of interest to us, τ is approximately half the spike width. Motivated by this discussion and by the fact that spike widths in real neurons are on the order of milliseconds, we set

$$\tau = 1$$

for the remainder of this article, think of time as measured in milliseconds, and always consider input currents $I \ll 1$.

2.2 Synapses Between Theta Neurons. We model synapses by adding time-dependent input currents to equation 2.1. When the presynaptic neuron spikes, the postsynaptic neuron receives an input current (positive or negative, depending on whether the synapse is excitatory or inhibitory), which jumps to its maximum value instantaneously and then decays exponentially. This is the model of section 2.1.5 of Izhikevich (2000) (see also Ermentrout, 1996, for a discussion of synapses between theta neurons).

---

increasing near the ghost of the equilibrium point. In this sense, V is more similar to $\sin\theta$ than to $-\cos\theta$.

Thus, a network of N coupled theta neurons is described by a system of differential equations of the form

$$\frac{d\theta_j}{dt} = 1 - \cos\theta_j + \left(I_j + \sum_{i=1}^{N} \alpha_i g_{ij} s_{ij}\right)(1 + \cos\theta_j), \quad 1 \le j \le N.$$

I_j denotes the external input to the jth neuron, which can be positive or negative. The constant α_i equals $+1$ or -1, depending on whether neuron i is excitatory (E) or inhibitory (I). The constant $g_{ij} \ge 0$ measures the strength of the synapse from neuron i to neuron j, and $s_{ij} = s_{ij}(t)$ is the synaptic gating variable associated with this synapse. The value of s_{ij} always lies between 0 and 1. It jumps to 1 when neuron i spikes. Between spikes of neuron i, it decays exponentially, following the differential equation

$$\frac{ds_{ij}}{dt} = -\frac{s_{ij}}{\tau_{ij}}.$$

The decay time constants τ_{ij} are positive.

The jumps of s_{ij} occurring when neuron i spikes cause difficulties in the numerical simulation of the network and are not physiologically realistic. In our simulations, we therefore replace the jumps by rapid but smooth rises, letting s_{ij} be governed by a differential equation of the form

$$\frac{ds_{ij}}{dt} = -\frac{s_{ij}}{\tau_{ij}} + e^{-\eta(1+\cos\theta_i)}\frac{1 - s_{ij}}{\tau_R},$$

with $\tau_R = 0.1$ and $\eta = 5$. The term $e^{-\eta(1+\cos\theta_i)}(1 - s_{ij})/\tau_R$ is very close to zero unless $\theta_i \approx (2l-1)\pi$, l integer, and drives s_{ij} toward 1 rapidly when $\theta_i \approx (2l-1)\pi$. The parameter τ_R is reminiscent of a synaptic rise time. Figure 3 shows s_{ij} for $\tau_{ij} = 2$ and 10, with the input of the presynaptic neuron chosen so that its period equals 25.

2.3 Sparse, Random E/I Networks. Throughout this article, the decay time constants τ_{ij} are assumed to depend on the type of i only (excitatory or inhibitory), so there are two distinct values of τ_{ij}, denoted τ_E and τ_I. We also assume that all excitatory neurons receive the same constant external input drive I_E, and all inhibitory neurons receive the same constant external drive I_I.

In later sections, we consider networks of coupled theta neurons, including $N_E = 4N/5$ excitatory and $N_I = N/5$ inhibitory neurons. These proportions are motivated by the fact that in large portions of the cortex, there are about four times more excitatory than inhibitory neurons (Braitenberg & Schüz, 1998).

The strengths g_{ij} of the synapses are chosen at random. For a given network, they are chosen once and for all; they do not depend on time. To de-

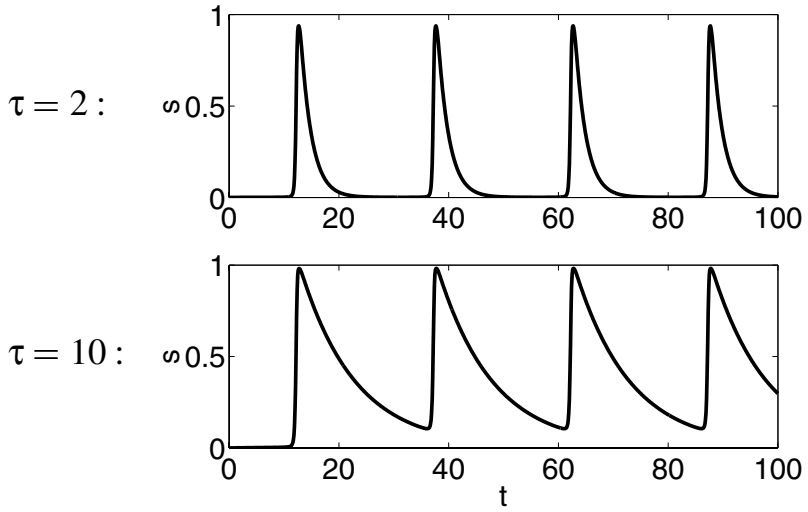

Figure 3: Synaptic gating variable s as a function of time, with decay time constants $\tau = 2$ and $\tau = 10$.

scribe the choice of the g_{ij}, the following notation is useful. Let $\mathcal{E} \subseteq \{1, \ldots, N\}$ denote the set of all indices of excitatory neurons, and similarly $\mathcal{I}$ the set of all indices of inhibitory neurons. For $i \in \mathcal{E}$ and $j \in \mathcal{I}$, we define

$$g_{ij} = \frac{g_{EI}}{p_{EI} N_E} w_{ij}, \tag{2.5}$$

with

$$w_{ij} = \begin{cases} 1 & \text{with probability } p_{EI}, \\ 0 & \text{otherwise,} \end{cases} \tag{2.6}$$

where $g_{EI} \geq 0$ and $p_{EI} \in (0, 1]$ are constants.

For $j \in \mathcal{I}$, we define

$$w_{Ej} = \sum_{i \in \mathcal{E}} w_{ij}. \tag{2.7}$$

Note that w_{Ej} is a binomially distributed random variable. We also define

$$g_{Ej} = \sum_{i \in \mathcal{E}} g_{ij} = \frac{g_{EI}}{p_{EI} N_E} w_{Ej}. \tag{2.8}$$

From the formulas for the mean and standard deviation of binomially distributed random variables, we see that g_{Ej} has mean g_{EI} and standard deviation

$$\sigma_{EI} = g_{EI}\sqrt{\frac{1-p_{EI}}{p_{EI}N_E}}. \tag{2.9}$$

By the central limit theorem, g_{Ej} is approximately normally distributed if $p_{EI}N_E$ is large. Assuming $p_{EI} \ll 1$, as is physiologically realistic (Braitenberg & Schüz, 1998), equation 2.9 shows that

$$\frac{\sigma_{EI}}{g_{EI}} \approx \frac{1}{\sqrt{p_{EI}N_E}}. \tag{2.10}$$

The left-hand side of equation 2.10 is the coefficient of variation (the standard deviation divided by the mean) of g_{Ej}, $j \in \mathcal{I}$. The expression $p_{EI}N_E$ appearing on the right-hand side is the expected number of excitatory inputs per I-cell.

Formulas analogous to 2.5 through 2.10 apply to the I $\to$ E, E $\to$ E, and I $\to$ I synapses. In particular,

$$\sigma_{IE} = g_{IE}\sqrt{\frac{1-p_{IE}}{p_{IE}N_I}}, \tag{2.11}$$

and therefore

$$\frac{\sigma_{IE}}{g_{IE}} \approx \frac{1}{\sqrt{p_{IE}N_I}} \tag{2.12}$$

for $p_{IE} \ll 1$. The left-hand side of equation 2.12 is the coefficient of variation of g_{Ij}, $j \in \mathcal{E}$. The expression $p_{IE}N_I$ appearing on the right-hand side is the expected number of inhibitory inputs per E-cell.

Several authors have pointed out that $p_{EI}N_E$ and $p_{IE}N_I$ are much more important than p_{EI}, N_E, p_{IE}, and N_I in isolation (Golomb & Hansel, 2000; Tiesinga, Fellous, José, & Sejnowski, 2002; Wang et al., 1995).

3 Loss of Tight Synchrony Is Attributable to Variance in the Number of Inputs per Cell

Before considering networks with sparse, random connectivity, we consider one with all-to-all connectivity ($p_{EI} = p_{IE} = 1.0$). Figure 1A shows an example of a simulation with

$$\begin{aligned} &I_E = 0.1, \quad I_I = 0, \quad g_{EI} = g_{IE} = 0.25, \\ &\quad g_{EE} = g_{II} = 0, \quad \tau_E = 2, \quad \tau_I = 10. \end{aligned} \tag{3.1}$$

Figure 1A shows spike times, with the horizontal axis indicating time and the vertical axis cell index. Each of the two cell groups (E and I) synchronizes very rapidly, with the synchronous population spikes of the I-cells slightly lagging behind those of the E-cells. The synchronization mechanism seen in Figure 1A is PING, briefly described in section 1 and discussed in more detail in section 6.1.

We comment briefly on our parameter choices. A neuron driven with $I_E = 0.1$ spikes periodically with an interspike interval equal to $\pi/\sqrt{I} \approx 9.93$. Since we think of time as measured in milliseconds, this corresponds to a frequency of (1000/9.93) H $\approx$ 100 Hz. Thus, the E-cells are driven so hard that they would spike above gamma frequency if they were not subject to any inhibition. The *I*-cells are driven at threshold; they do not spike without additional excitatory input, but any excitatory input, regardless how weak, will make them spike. The values of g_{EI} and g_{IE} can be varied considerably without any qualitative change in Figure 1A. However, for small values of g_{EI} (roughly < 0.1), two or more population spikes of the E-cells occur before the I-cells respond. For large values of g_{EI} (roughly > 0.7), two or more population spikes of the I-cells occur in response to a population spike of the E-cells. For small values of g_{IE} (roughly < 0.1), the E-cells are not synchronized. For large values of g_{IE}, the rhythm is slow but not qualitatively different from that in Figure 1A. For simplicity, we assume here that there are no E $\rightarrow$ E or I $\rightarrow$ I synapses—$g_{EE} = g_{II} = 0$. In our experience, E $\rightarrow$ E synapses (with a brief synaptic decay time such as $\tau_E = 2$) do not affect PING rhythms much. However, I $\rightarrow$ I synapses are crucial in some parameter regimes; this will be discussed in section 6.1. Our choices of $\tau_E = 2$ and $\tau_I = 10$ are motivated by the decay time constants of excitatory synapses involving AMPA receptors (approximately 2 ms) and inhibitory synapses involving $GABA_A$ receptors (approximately 10 ms); recall that we think of time as measured in milliseconds.

When p_{EI} and p_{IE} are reduced from 1.0 to 0.5, Figure 1A turns into Figure 1B. The two cell groups now fire spike volleys of positive durations. As stated in section 1, the main goal of this article is to understand the durations and shapes of these volleys.

In the network underlying Figure 1B, each E-cell receives input from a random number of I-cells. The expected value of this number is 50. Similarly, each I-cell receives input from a random number of E-cells, with expectation 200. We now repeat the simulation of Figure 1B with a network in which the connectivity is still sparse and random, but the variance in the number of inputs per cell has been eliminated. That is, each E-cell receives input from a random set of exactly 50 I-cells, and each I-cell receives input from a random set of exactly 200 E-cells. The network is like that of Figure 1B in all other regards. The result is shown in Figure 4A; tight synchrony is restored.

When the number of inputs per cell is fixed, tight synchronization is possible even for much sparser networks. Figure 4B shows a simulation

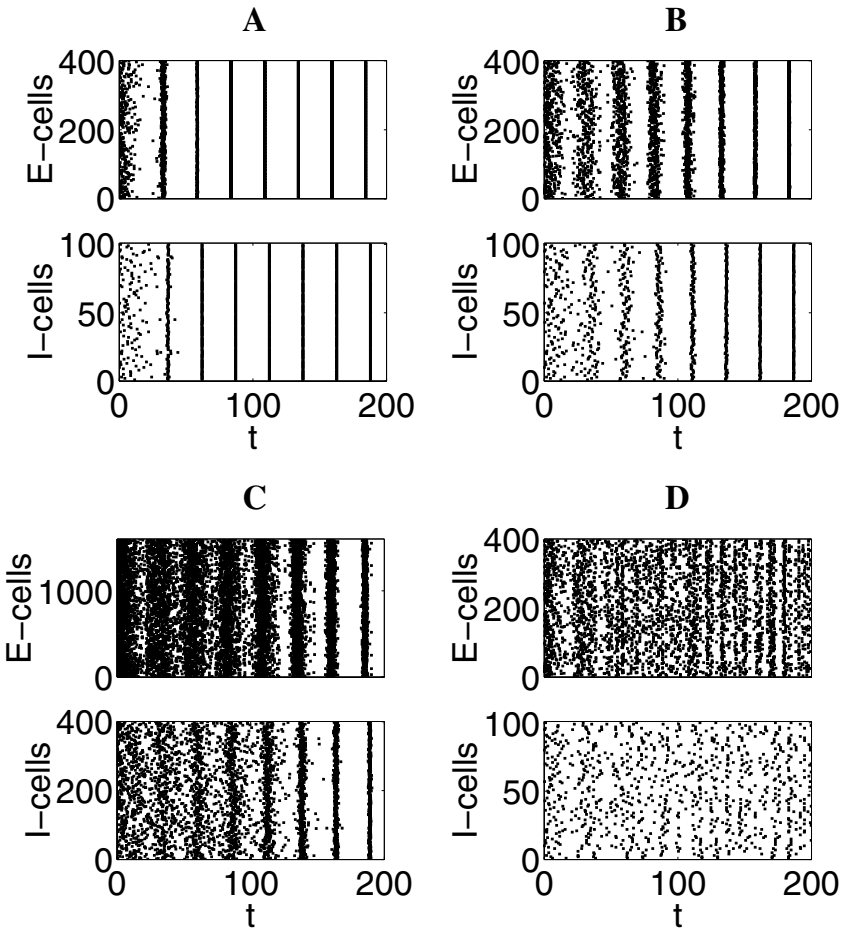

Figure 4: Simulation of E-I networks with sparse, random connectivity but without variance in the number of inputs per cell. (A) Parameters as in Figure 1B, but with variance in numbers of inputs per cell eliminated. (B) Only four excitatory inputs per I-cell and one inhibitory input per E-cell. (C) Same as *B* in a larger network. (D) Same as *B*, but with only one excitatory input per I-cell.

in which each E-cell receives input from one I-cell, and each I-cell receives input from four E-cells. Although synchronization is achieved a little less rapidly than in Figure 4A, it becomes tight within a few oscillation periods. A four times larger network, again with one inhibitory input into each E-cell and four excitatory inputs into each I-cell, shows similar behavior (see Figure 4C).

If the number of excitatory inputs per I-cell is reduced again, from four to one, there appears to be no more synchronization (see Figure 4D). Thus, there appears to be a minimum number of inputs per cell needed for synchronization—a "percolation threshold." However, this number is very small in our simulations. In previous work on different models, similar thresholds have been found (Golomb & Hansel, 2000; Wang & Buzsáki, 1996; Wang et al., 1995). In all three of these references, asynchrony was found to become unstable when the number of inputs per cell exceeded a threshold value independent of network size.

A cell in a human brain typically receives input from thousands of other cells (Braitenberg & Schüz, 1998). Our numerical experiments suggest that with so many synapses, the impact of sparse, random connectivity on synchronization is attributable to the variance in the number of inputs per cell, not to the percolation threshold. We will assume this to be the case from now on.

4 Synchronization of a Population of Theta Neurons by a Single Strong Inhibitory Pulse

4.1 Synchronization by an Inhibitory Pulse of Uniform Strength. We consider a population of N identical, uncoupled neurons with common constant external drive above threshold, receiving a common inhibitory synaptic input pulse at time 0. Following section 2, we model this population by the equations

$$\frac{d\theta_j}{dt} = (1 - \cos\theta_j) + (I - gs(t))(1 + \cos\theta_j), \qquad 1 \le j \le N, \tag{4.1}$$

with $I > 0$, $g > 0$, and

$$s(t) = \begin{cases} e^{-t/\tau_I} & \text{if } t > 0 \\ 0 & \text{if } t \le 0 \end{cases}$$

with $\tau_I > 0$. If the inhibitory pulse is strong, it brings the population close to synchrony. An example is shown in Figure 5A, which displays results of a simulation with

$$N = 100, \quad I = 0.05, \quad g = 0.25, \quad \tau_I = 10. \tag{4.2}$$

The synchronization brought about by the inhibitory pulse at time 0 is immediate and nearly perfect.

To understand the synchronization shown in Figure 5A, consider the initial value problem,

$$\frac{d\theta}{dt} = 1 - \cos\theta + (I - ge^{-t/\tau_I})(1 + \cos\theta), \quad t > 0, \tag{4.3}$$

$$\theta(0) = \theta_0, \tag{4.4}$$

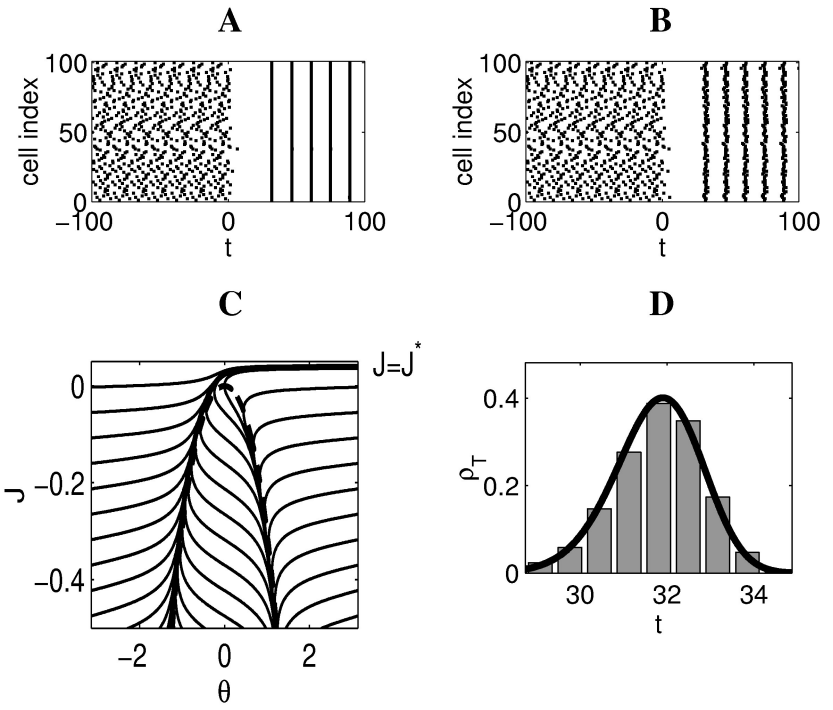

Figure 5: Synchronization by a single inhibitory pulse. (A) Inhibitory pulse of uniform strength. (B) Inhibitory pulse of nonuniform strength. (C) Phase portrait for equations 4.5 and 4.6 with $I = 0.05$, $\tau_I = 10$, with the stable river indicated boldly. (D) Distribution of spikes within the first volley following $t = 0$, in a simulation identical to that in B, but with 1000 neurons: predicted (solid line) and actual (bars).

with $-\pi < \theta_0 < \pi$. We define

$$J(t) = I - ge^{-t/\tau_I}.$$

Equations 4.3 and 4.4 can then be rewritten in the form

$$\frac{d\theta}{dt} = 1 - \cos\theta + J(1 + \cos\theta) \tag{4.5}$$

$$\frac{dJ}{dt} = -\frac{J - I}{\tau_I} \tag{4.6}$$

$$\theta(0) = \theta_0 \tag{4.7}$$

$$J(0) = I - g. \tag{4.8}$$

The phase portrait for the two-dimensional dynamical system 4.5 and 4.6 is shown in Figure 5C for $I = 0.05$ and $\tau_I = 10$. The dashed line in Figure 5C is the nullcline $d\theta/dt = 0$. The nullcline $dJ/dt = 0$ is the horizontal line $J = I$, the upper edge of the window shown in Figure 5C. The figure should be extended periodically in θ with period 2π. The flow is upward, in the direction of increasing J.

The most striking feature of Figure 5C is the existence of strongly attracting and strongly repelling trajectories. Trajectories of this kind exist in many systems of ordinary differential equations and are called rivers (Diener, 1985a, 1985b). The figure reveals a stable river, that is, a trajectory (θ_s, J_s) that is attracting in forward time, indicated as a bold line in Figure 5C, with $(\theta_s, J_s) \to (-\pi, -\infty)$ as $t \to -\infty$, $d\theta_s/dt > 0$, and

$$J_s(t) = I - ge^{-t/\tau_I} \tag{4.9}$$

for all t. We denote by T the time when $\theta_s(T) = \pi$, and define

$$J^* = J_s(T) \in (0, I). \tag{4.10}$$

Equations 4.9 and 4.10 imply

$$T = \tau_I \ln g - \tau_I \ln(I - J^*). \tag{4.11}$$

Note that the phase portrait depends on the parameters I and τ_I but not on g. Therefore, the value of J^* depends on I and τ_I but not on g.

The synchronization seen in Figure 5A can be understood from Figure 5C in the following way. For g sufficiently large (that is, $J(0)$ sufficiently negative), and for θ_0 sufficiently far from π, $(\theta(t), J(t))$ is rapidly attracted to $(\theta_s(t), J_s(t))$. At the time when $\theta = \pi$, we therefore have $J \approx J^*$ or $t \approx T$. Thus, the first spike after time zero occurs approximately at time T. For θ_0 sufficiently close to π, $\theta(t)$ quickly passes through π and is then rapidly attracted to $(\theta_s(t) + 2\pi, J_s(t))$. When $\theta(t)$ reaches 3π, $J \approx J^*$ and therefore $t \approx T$. Thus, a spike occurs soon after time zero, followed by a spike approximately at time T. Only for values of θ_0 in a narrow transition regime is $(\theta(t), J(t))$ attracted to neither $(\theta_s(t), J_s(t))$ nor $(\theta_s(t) + 2\pi, J_s(t))$.

Equation 4.11 gives the time of the first approximately synchronous population spike. Since we have no explicit formula for J^*, equation 4.11 is not an explicit formula for T. However, since J^* does not depend on g, equation 4.11 does give the precise dependence of T on g. This dependence will be of primary interest to us in the remainder of section 4. For later reference, we note how equation 4.11 is modified when the synchronizing inhibitory pulse arrives not at time 0 but at some time T_0:

$$T = T_0 + \tau_I \ln g - \tau_I \ln(I - J^*). \tag{4.12}$$

4.2 Approximate Synchronization by an Inhibitory Pulse of Nonuniform Strength. Motivated by section 3, we are interested in the effects of variable synaptic strengths. We therefore let the constant g in equation 4.1 depend on j:

$$\frac{d\theta_j}{dt} = (1 - \cos\theta_j) + (I - g_j s(t))(1 + \cos\theta_j), \qquad 1 \le j \le N.$$

That is, different neurons receive inhibitory pulses of different strengths. We assume that the g_j are independent, normally distributed random variables, with mean $\overline{g} > 0$ and standard deviation $\sigma_g > 0$. If $\overline{g}$ is large enough and σ_g is small enough, the population is still synchronized approximately. This is illustrated in Figure 5B, which shows results of a simulation similar to that of Figure 5A, with

$$N = 100, \quad I = 0.05, \quad \overline{g} = 0.25, \quad \sigma_g = 0.025, \quad \tau_I = 10. \tag{4.13}$$

(Compare these parameters with those in equations 4.2.) Instead of the nearly synchronous population spikes of Figure 5A, we now see spike volleys of brief but positive durations.

To analyze the durations of these spike volleys, let us consider the initial value problem 4.3 and 4.4 with a random $g > 0$. Let $\rho_g = \rho_g(\gamma)$, $\gamma > 0$ be the probability density of g, and let $\overline{g} > 0$ and $\sigma_g > 0$ be its mean and standard deviation. Let

$$X = \ln g. \tag{4.14}$$

Combining equations 4.11 and 4.14,

$$T = \tau_I X - \tau_I \ln(I - J^*). \tag{4.15}$$

The only random quantity on the right-hand side of equation 4.15 is X. We will discuss its distribution first. Let $\rho_X = \rho_X(\xi)$, $-\infty < \xi < \infty$ be the probability density of X. For $-\infty < a < b < \infty$,

$$\int_a^b \rho_X(\xi)\, d\xi = P(X \in (a,b)) = P(\ln g \in (a,b)) = P(g \in (e^a, e^b))$$

$$= \int_{e^a}^{e^b} \rho_g(\gamma)\, d\gamma = \int_a^b e^\xi \rho_g(e^\xi)\, d\xi.$$

Therefore,

$$\rho_X(\xi) = e^\xi \rho_g(e^\xi) \tag{4.16}$$

for all ξ. For small σ_g, the standard deviation of X is

$$\sigma_X \approx \ln'(\overline{g})\sigma_g = \frac{\sigma_g}{\overline{g}}. \tag{4.17}$$

From equations 4.15 and 4.16, we see that the probability density function of T is

$$\rho_T(t) = \frac{1}{\tau_I} e^{(t+\tau_I \ln(I-J^*))/\tau_I} \rho_g(e^{(t+\tau_I \ln(I-J^*))/\tau_I}). \tag{4.18}$$

For later reference, we note how formula 4.18 changes if the approximately synchronizing inhibitory pulse arrives not at time 0 but at some time T_0:

$$\rho_T(t) = \frac{1}{\tau_I} e^{(t-T_0+\tau_I \ln(I-J^*))/\tau_I} \rho_g(e^{(t-T_0+\tau_I \ln(I-J^*))/\tau_I}). \tag{4.19}$$

Using equations 4.15 and 4.17, we see that the standard deviation of T is

$$\sigma_T = \tau_I \sigma_X \approx \tau_I \frac{\sigma_g}{\overline{g}} \tag{4.20}$$

for small σ_g. We think of σ_T as a measure of the duration of the spike volleys. Thus, the duration of the spike volleys is proportional to the product of τ_I, the decay time constant of inhibition, and the coefficient of variation $\sigma_g/\overline{g}$ of g.

To verify these results computationally, we return to the example of Figure 5B. Strictly speaking, the preceding discussion does not apply to this example, since g, which is assumed to be normally distributed, is not guaranteed to be positive. However, formulas 4.16, 4.18, and 4.20 are well defined if ρ_g is a normal density. Since $\overline{g} = 0.25$ and $\sigma_g = 0.025$, the probability of $g \leq 0$ is extremely small. We therefore expect equations 4.16, 4.18, and 4.20 to hold with good accuracy.

We define $T^{(j)}$ to be the time of the spike of the jth neuron within the first nearly synchronous spike volley. We set

$$\hat{\overline{T}} = \frac{\sum_{j=1}^{N} T^{(j)}}{N} \quad \text{and} \quad \hat{\sigma}_T = \sqrt{\frac{\sum_{j=1}^{N} (T^{(j)} - \hat{\overline{T}})^2}{N-1}}. \tag{4.21}$$

Here and for the remainder of this article, hats indicate results obtained from numerical simulations. In the example of Figure 5B, we find

$$\hat{\sigma}_T \approx 1.02.$$

We see that $\hat{\sigma}_T$ is indeed close to $\tau_I \sigma_g/\overline{g}$, which equals 1.0 in this example. If we double τ_I in this experiment, $\hat{\sigma}_T$ rises from 1.02 to 2.04, in agreement with equation 4.20.

To verify equation 4.18 numerically, we must know the value of $\tau_I \ln(I - J^*)$. Taking expectations on both sides of equation 4.15, we find

$$\tau_I \ln(I - J^*) = \tau_I E(X) - E(T) = \tau_I E(\ln g) - E(T).$$

For sufficiently small σ_g, this implies

$$\tau_I \ln(I - J^*) \approx \tau_I \ln \overline{g} - E(T),$$

suggesting the approximation

$$\tau_I \ln(I - J^*) \approx \tau_I \ln \overline{g} - \hat{\overline{T}}. \tag{4.22}$$

Figure 5D shows the density ρ_T, as defined in equation 4.18, using the approximation 4.22, with $\tau_I = 10$, and assuming that ρ_g is a normal density with $\overline{g} = 0.25$ and $\sigma_g = 0.025$. The histogram in Figure 5D indicates the actual spike time density, determined from the numerical simulation. The agreement between the theoretical prediction and the actual spike time distribution is excellent.

For later reference, we note how equation 4.22 changes when the inhibitory pulse arrives not at time 0 but at some time T_0. From equation 4.12, we then obtain

$$\tau_I \ln(I - J^*) \approx \tau_I \ln \overline{g} + T_0 - \hat{\overline{T}}. \tag{4.23}$$

5 Synchronization of a Population of Theta Neurons by a Single Strong Excitatory Pulse

5.1 The Synchronous Population Spike Triggered by an Excitatory Pulse of Uniform Strength. We next consider a population of N identical, uncoupled neurons with common constant external drive below or at threshold, receiving a common excitatory synaptic input pulse at time 0. We model this situation by the equations

$$\frac{d\theta_j}{dt} = (1 - \cos\theta_j) + (I + gs(t))(1 + \cos\theta_j), \qquad 1 \le j \le N, \tag{5.1}$$

with $I \le 0$, $g > 0$, and

$$s(t) = \begin{cases} e^{-t/\tau_E} & \text{if } t > 0 \\ 0 & \text{if } t \le 0 \end{cases}$$

with $\tau_E > 0$. If the excitatory pulse is strong, it triggers a nearly synchronous population spike soon after time 0.

To analyze this in more detail, we consider the initial value problem:

$$\frac{d\theta}{dt} = 1 - \cos\theta + (I + ge^{-t/\tau_E})(1 + \cos\theta), \qquad t > 0, \tag{5.2}$$

$$\theta(0) = -2 \arccos \frac{1}{\sqrt{1 - I}}. \tag{5.3}$$

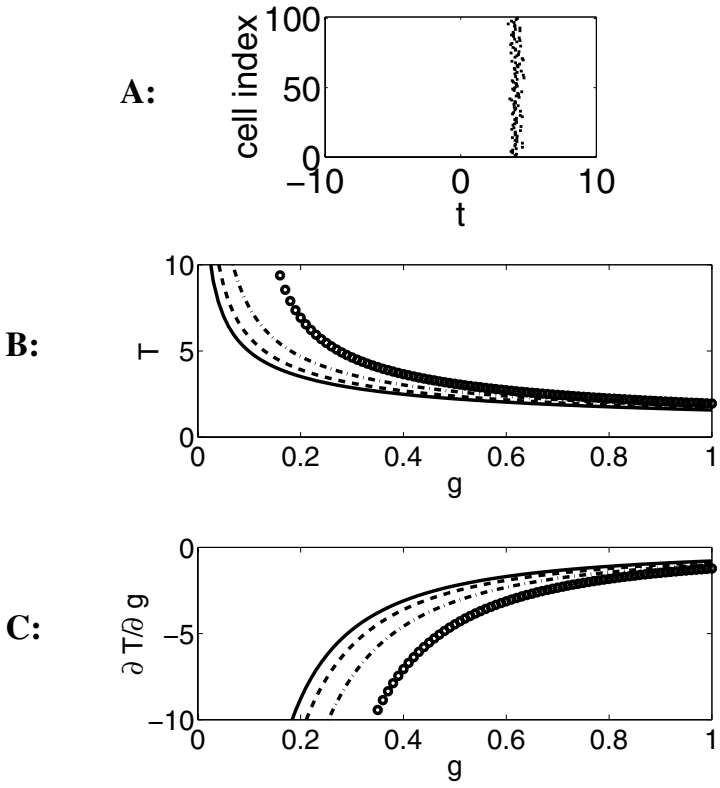

Figure 6: (A) Approximately synchronous population spike triggered by a single nonuniform excitatory pulse. (B) Time T between arrival of excitatory pulse and spike triggered by it, as a function of the strength g of the pulse, for (I, τ_E)=$(0, \infty)$ (solid line), $(0, 5)$ (dashed line), $(0, 2)$ (dash-dotted line), $(-0.01, 2)$ (circles). (C) $\partial T/\partial g$ as a function of g, for the parameter values of B.

Recall from section 2 that for $I < 0$, the right-hand side of equation 5.3 represents the stable fixed point of the equation $d\theta/dt = 1 - \cos\theta + I(1 + \cos\theta)$. Thus, we are considering the response of a neuron at rest to an excitatory synaptic pulse. We denote by T the first time at which the neuron spikes, with $T = \infty$ if there is no spike at all.

We have no general analytic expression for T as a function of I, τ_E, and g. However, it is easy to see that for fixed I and τ_E, T is a strictly decreasing function of g, with $\lim_{g\to\infty} T = 0$ and $\lim_{g\to g_c+} T = \infty$ for some $g_c \geq 0$ (see Figure 6B). For $\tau_E = \infty$, T can be computed using formula 2.2, with I

replaced by $I + g$ and $\tau = 1$. The formula becomes particularly simple for $I = 0$; in that case,

$$T = \frac{\pi}{2}\frac{1}{\sqrt{g}}. \tag{5.4}$$

The approximation $\tau_E = \infty$ is accurate as long as $e^{-T/\tau_E} \approx 1$, since then the exponential decay in equation 5.2 can be neglected over the time interval $[0, T]$. Since $T \to 0$ as $g \to \infty$, this means that the assumption $\tau_E = \infty$ is accurate for sufficiently large g. The assumption $I = 0$ is accurate when $|I|/g$ is sufficiently small. So this assumption too is accurate for sufficiently large g.

Figure 6B shows T as a function of g, for various values of I and τ_E, demonstrating that equation 5.4 approximates T reasonably well over a large range of parameter values.

5.2 The Approximately Synchronous Population Spike Triggered by an Excitatory Pulse of Nonuniform Strength. If the synaptic strength in equation 5.1 depends on j, that is, if different neurons receive excitatory pulses of different strengths, the equations are

$$\frac{d\theta_j}{dt} = (1 - \cos\theta_j) + (I + g_j s(t))(1 + \cos\theta_j), \qquad 1 \le j \le N.$$

Figure 6A shows that the resulting population spike is not perfectly synchronous. (But notice that Figure 6A shows a brief time window only; the synchronization is not perfect but fairly tight.) In the simulation underlying this figure,

$$N = 100, \quad I = 0, \quad \overline{g} = 0.25, \quad \sigma_g = 0.025, \quad \tau_E = 2. \tag{5.5}$$

To analyze the duration of the spike volley triggered by an excitatory pulse of nonuniform strength, we consider the initial value problem 5.2, 5.3 with a random $g > g_c$. If σ_g is small, the standard deviation of T is

$$\sigma_T \approx \left|\frac{\partial T}{\partial g}\right| \sigma_g. \tag{5.6}$$

For $\tau_E = \infty$ and $I = 0$,

$$\frac{\partial T}{\partial g} = \frac{\pi}{4} g^{-3/2} \tag{5.7}$$

by equation 5.4. Figure 6C shows $\partial T/\partial g$ as a function of g, for various values of I and τ_E. The figure confirms that the right-hand side of equation 5.7 approximates $\partial T/\partial g$ reasonably well for large values of g. Combining equations 5.6 and 5.7 yields

$$\sigma_T \approx \frac{\pi}{4}\frac{1}{\sqrt{\overline{g}}}\frac{\sigma_g}{\overline{g}}. \tag{5.8}$$

For illustration, we return to the example of Figure 6A ($I = 0$, $\tau_E = 2$, $\overline{g} = 0.25$, $\sigma_g = 0.025$). We define $T^{(j)}$ to be the time of the spike of the jth neuron, and define $\hat{\overline{T}}$ and $\hat{\sigma}_T$ as in equation 4.21. Numerically, we find

$$\hat{\sigma}_T \approx 0.270.$$

To evaluate the right-hand side of equation 5.6, we approximate $\partial T/\partial g$ numerically. We find $\partial T/\partial g \approx -10.30$ for the parameter values of Figure 6A. The approximation of equation 5.6, based solely on the assumption that σ_g is so small that the relation between σ_T and σ_g is approximately linear, proves fairly accurate here; it yields

$$\sigma_T \approx 0.256.$$

The assumption $\tau_E = \infty$, which underlies equation 5.8, degrades the accuracy, but by less than a factor of two:

$$\sigma_T \approx 0.157.$$

6 The PING Synchronization Mechanism

6.1 PING in Fully Connected E-I Networks. We return to the example of Figure 1A. Each of the cell groups (E and I) synchronizes rapidly, with the population spikes of the inhibitory neurons slightly lagging behind those of the excitatory ones. We state, in a nonrigorous way, based on numerical experience and heuristics, conditions that are sufficient to induce firing patterns as in Figure 1A:

Condition 1: The E-cells receive external input significantly above their spiking threshold.

Condition 2: The E $\rightarrow$ I synapses are so strong and have so short a rise time that a surge in spiking of the E-cells quickly triggers a surge in spiking of the I-cells.

Condition 3: The I-cells spike only in response to the E-cells.

Condition 4: The I $\rightarrow$ E synapses are so strong that a population spike of the I-cells approximately synchronizes the E-cells.

If these four conditions are satisfied, synchronous rhythmic spiking develops as follows (Whittington et al., 2000; Tiesinga et al., 2001). Initial activity in the E-cells triggers activity in the I-cells. This inhibits activity in the E-cells, thereby removing the drive to the I-cells. A period of low activity in both E- and I-cells results. When the inhibition wears off and the E-cells spike again, they are closer to synchrony than previously because of the mechanism described in section 4.1. The spiking of the E-cells causes spiking of the I-cells, closer to synchrony than previously because of the mechanism of section 5.1. The cycle now repeats.

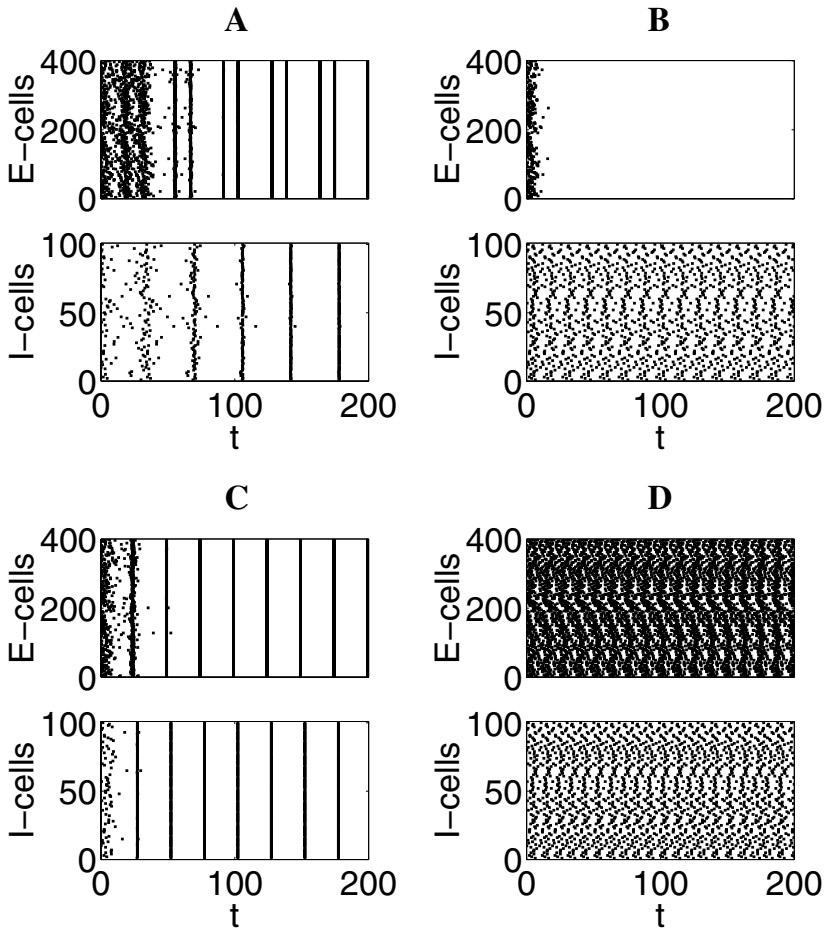

Figure 7: Illustration of conditions 2–4 from section 6.1. (A) PING is lost when E → I synapses become too weak. (B) PING is lost as a result of too much drive to the I-cells. (C) Rhythm is restored by adding I → I synapses. (D) PING is lost when I → E synapses become too weak.

Condition 1 is evidently needed to drive activity. We discuss conditions 2 through 4 in more detail and present numerical results illustrating what happens when they are violated.

When condition 2 is violated, that is, when the E → I synapses are weak, a pattern such as the one shown in Figure 7A often develops: the E-cells and the I-cells still synchronize, but the E-cells spike several times between population spikes of the I-cells. The parameters in Figure 7A are as in Figure 1A, except that g_{EI} has been reduced from 0.25 to 0.05.

Condition 3 is violated if the drive to the I-cells becomes too strong, but can be restored by introducing I $\rightarrow$ I-synapses. We illustrate this with the following numerical experiment. In Figure 1A, $I_I = 0$. If we raise I_I to 0.05, the figure changes dramatically, as shown in Figure 7B. Here, I_I is strong enough to drive asynchronous activity in the I-cells that suppresses the E-cells altogether. Condition 3, and with it the rhythm, is restored by setting $g_{II} = 0.25$ (see Figure 7C).

We note that in the example of Figure 7C, the I-cells would spike synchronously even without the E-cells. Thus, the role of the I-I synapses is to synchronize the I-cells, replacing nearly constant inhibition by phasic inhibition, which allows the E-cells to fire. One might therefore consider the rhythm in Figure 7C an "ING" or "γ-I" rhythm (see section 7). The parameter regime investigated here is similar to that of Figure 7d of Tiesinga et al. (2001). There as here, asynchronous activity of the I-cells suppresses activity in the E-cells altogether, while synchronous activity of the I-cells permits firing of the E-cells. However, in Figure 7C, the E-cells do play an important role in setting the frequency of the rhythm. In the absence of the E-cells, the rhythm would be much slower. Thus, the firing of the I-cells in Figure 7C does come in response to the firing of the E-cells, as in PING.

Figure 7D shows what may happen when condition 4 is violated, that is, when the I $\rightarrow$ E synapses are weak. The parameters in Figure 7D are as in Figure 1A, except that g_{IE} has been reduced from 0.25 to 0.05. The inhibitory synapses no longer suffice to synchronize the E-cells. As a result, the I-cells, which were synchronized by the E-cells in Figure 1A, are no longer synchronized either.

A mathematical examination of conditions 1 through 4 will be the subject of future publications.

6.2 PING in Sparsely, Randomly Connected E-I Networks. When p_{EI} and p_{IE} are reduced from 1.0 to 0.5, Figure 1A turns into Figure 1B. In analyzing the population spikes of the E-cells in Figure 1B, we make the simplifying assumption that the population spikes of the I-cells are perfectly synchronous. Since the I-cells are in fact fairly tightly synchronized in Figure 1B, this is a good approximation at least for the parameters used in Figure 1B. When the I-cells spike, all E-cells receive inhibitory pulses. However, different neurons receive inputs of different strengths because of the random connectivity. The resulting approximately synchronous spike volley of the E-cells can be analyzed using section 4.2.

We focus on one particular spike volley of the E-cells, say, the first one following $t = 100$ in Figure 1B. We define $T_E^{(j)}$ to be the time of the spike of the jth E-cell during this volley. We define

$$\hat{\overline{T}}_E = \frac{\sum_j T_E^{(j)}}{N_E} \quad \text{and} \quad \hat{\sigma}_E = \sqrt{\frac{\sum_j (T_E^{(j)} - \hat{\overline{T}}_E)^2}{N_E - 1}}.$$

From equations 2.11 and 4.20, we find the prediction

$$\hat{\sigma}_E \approx \tau_I \sqrt{\frac{1-p_{IE}}{p_{IE}N_I}}. \tag{6.1}$$

For the first spike volley of the E-cells following $t = 100$ in Figure 1B, we find numerically

$$\hat{\sigma}_E = 1.18.$$

The prediction of equation 6.1 is remarkably accurate:

$$\tau_I \sqrt{\frac{1-p_{IE}}{p_{IE}N_I}} \approx 1.22.$$

We expect the shape of the spike volley to be approximately described by equation 4.19. To evaluate equation 4.19, we must evaluate $T_0 - \tau_I \ln(I - J^*)$. (Recall that T_0 is the time at which the synchronizing inhibitory pulse arrives, here the time of the inhibitory population spike immediately preceding the excitatory population spike under consideration.) Following equation 4.23, we use the approximation

$$T_0 - \tau_I \ln(I - J^*) \approx \hat{\overline{T}}_E - \tau_I \ln g_{IE}.$$

The predicted and actual spike time distributions are shown in Figure 8. The agreement is good.

We now consider the first spike volley of the I-cells following $t = 100$ in Figure 1B. We define $T_I^{(j)}$ to be the time of the spike of the jth I-cell during this volley, and

$$\hat{\overline{T}}_I = \frac{\sum_j T_I^{(j)}}{N_I} \quad \text{and} \quad \hat{\sigma}_I = \sqrt{\frac{\sum_j (T_I^{(j)} - \hat{\overline{T}}_I)^2}{N_I - 1}}.$$

From equations 2.9 and 5.8, we find the prediction

$$\hat{\sigma}_I \approx \frac{\pi}{4} \frac{1}{\sqrt{g_{EI}}} \sqrt{\frac{1-p_{EI}}{p_{EI}N_E}}. \tag{6.2}$$

For the first spike volley of the I-cells following $t = 100$ in Figure 1B, we find numerically

$$\hat{\sigma}_I = 0.151.$$

The prediction of equation 6.2 is somewhat inaccurate, as was to be expected, because it is based on three rather substantial idealizations: $\tau_E = \infty$, perfect

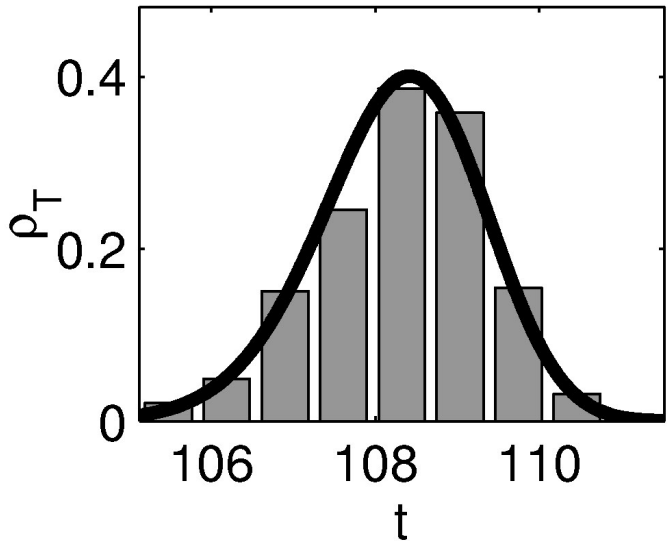

Figure 8: Distribution of spikes within the first spike volley following $t = 100$ in Figure 1B: predicted (solid line) and actual (bars).

synchrony of the E-cells, and the assumption that the I-cells return to rest between the spike volleys of the E-cells (see equation 5.3). However, the discrepancy is still not greater than a factor of two:

$$\frac{\pi}{4}\frac{1}{\sqrt{g_{EI}}}\sqrt{\frac{1-p_{EI}}{p_{EI}N_E}} \approx 0.0785.$$

We note that it would be possible to relax the assumption of perfect synchrony in the E-cells, since we have fairly precise information about the durations and even the shapes of the spike volleys of the E-cells. We do not pursue this here, since our goal here is qualitative insight, not precise quantitative information.

7 Discussion

We have analyzed the effects of sparse, random connectivity on the PING synchronization mechanism. In particular, we have derived approximate formulas for the durations of the spike volleys, equations 6.1 and 6.2. To make these formulas as transparent as possible, let us use the approximations $1 - p_{IE} \approx 1$ and $1 - p_{EI} \approx 1$, and write

$$M_{EI} = p_{EI}N_E$$

for the expected number of excitatory inputs per inhibitory cell and

$$M_{IE} = p_{IE} N_I$$

for the expected number of inhibitory inputs per excitatory cell. Equations 6.1 and 6.2 then become

$$\hat{\sigma}_E \approx \tau_I \frac{1}{\sqrt{M_{IE}}} \tag{7.1}$$

and

$$\hat{\sigma}_I \approx \frac{\pi}{4\sqrt{g_{EI}}} \frac{1}{\sqrt{M_{EI}}}. \tag{7.2}$$

An interesting feature of these formulas is their lack of symmetry. The time constant τ_I appears in equation 7.1, but the time constant τ_E does not appear in equation 7.2. Similarly, g_{EI} appears in equation 7.2, but g_{IE} does not appear in equation 7.1.

If a theta neuron were driven with a constant drive equal to g_{EI}, it would spike periodically with a period which we call P_{EI}. From equation 2.3,

$$P_{EI} = \frac{\pi}{\sqrt{g_{EI}}}.$$

Using this in equation 7.2, we find

$$\hat{\sigma}_I \approx \frac{1}{4} \frac{P_{EI}}{\sqrt{M_{EI}}}. \tag{7.3}$$

Let P denote the period of the PING rhythm. In the simulations of this article,

$$P_{EI} \ll \tau_I < P, \quad M_{EI} > M_{IE} \gg 1. \tag{7.4}$$

The inequality $M_{IE} \gg 1$ is certainly realistic (Braitenberg & Schüz, 1998). The inequality $\tau_I < P$ holds for a gamma rhythm if the inhibitory synapses are mediated by $GABA_A$, since the typical period of gamma oscillations is about 25 ms and the decay time constant of $GABA_A$ synapses is about 10 ms. It appears that PING without $P_{EI} \ll \tau_I$ is not possible with realistic values of τ_I; more will be said on this point. Combining 7.1, 7.3, and 7.4, we find

$$\hat{\sigma}_I \ll \hat{\sigma}_E \ll P.$$

Thus, our theory predicts that for PING in realistic parameter regimes, sparse and random connectivity will not prevent either E- or I-cells from synchronizing fairly tightly, but the I-cells will synchronize much more tightly

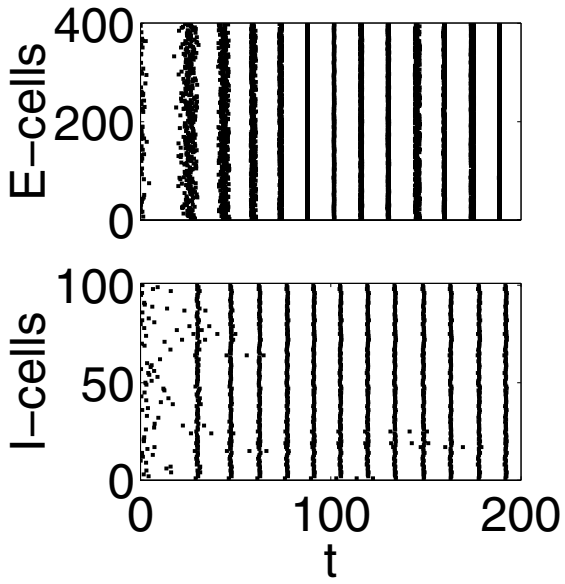

Figure 9: PING in an E-I network with sparse, random connectivity, with nearly instantaneous synapses.

than the E-cells. Our computational results are in agreement with these conclusions (see Figure 1B).

It is possible to obtain PING without the condition $P_{EI} \ll \tau_I$ if τ_I is made unrealistically small. To compensate, one must then also make g_{IE} unrealistically large. In fact, in many modeling studies, synapses have been assumed to act instantaneously, that is, with zero rise and decay times (Brunel, 2000; Brunel & Hakim, 1999; Izhikevich, 1999; Mirollo & Strogatz, 1990; Tiesinga & Sejnowski, 2001); this amounts to taking a limit in which simultaneously $\tau_I \to 0$ and $g_{IE} \to \infty$. (In Brunel, 2000, and Brunel & Hakim, 1999, there is a delay between the spiking of the presynaptic neuron and its effect on the postsynaptic neuron; however, this delay is not relevant for this discussion.) In some regard, the behavior of instantaneous synapses is not very different from that of synapses with more realistic time courses. However, equations 7.1 and 7.2 predict that the effects of random connectivity will be reduced dramatically by making the synapses instantaneous. To verify this numerically, we repeat the simulation of Figure 1B, with τ_I reduced by a factor of 50 and g_{IE} raised by a factor of 50. This closely mimics instantaneous synapses but is computationally simpler. The result is shown in Figure 9. As predicted, synchronization is much tighter than in Figure 1B, even though the randomness in the connectivity is the same in Figure 9 as in Figure 1B. The rhythm is also accelerated; this is a result of the reduction in τ_I.

Our theory for the spike volleys of the E-cells is precise enough to allow accurate predictions not just of the durations of the volleys but even of their shapes, as shown in Figure 8. A refinement of the theory could be obtained by taking into account the positive durations of the spike volleys of the I-cells, perhaps using ideas similar to those of section 3.2 of Tiesinga and Sejnowski (2001). (Recall that in section 4, the duration of the spike volleys of the I-cells was assumed to be negligible.) However, our numerical results indicate that in our parameter regime, neglecting the durations of the spike volleys of the I-cells gives an excellent approximation. Tiesinga et al. (2002) discuss a related problem, using numerical simulation primarily, and with an emphasis on information-theoretic ideas. They also present experimental results. For instance, Figure 8b of their article illustrates how the jitter in the spike times of a rat hippocampal neuron decreases when the quantity n_{pre} (our $p_{IE}N_I$) increases, in rough qualitative agreement with equation 6.1. (Rough qualitative agreement is the best that can be expected here, in view of the idealized nature of our theory.)

Our theory for the spike volleys of the I-cells is less accurate than that for the excitatory ones. However, since the synchronization of the I-cells is typically quite tight and brought about by a crude mechanism (a burst of excitation triggers an almost immediate, and therefore almost synchronous, response of the I-cells), a precise theory for the spike volleys of the I-cells is of less interest here. To create such a theory, we would need to study how the duration of an excitatory input spike volley is related to the duration of an output spike volley triggered by it. (Recall that in section 5, the duration of the spike volleys of the E-cells was assumed to be negligible.) This issue is centrally important in the study of synfire chains (Diesmann, Gewaltig, & Aertsen, 1999). Figure 3c of Diesmann et al. (1999) shows that the strength of the input spike volley is crucial. Strong, loosely synchronous input spike volleys can trigger tightly synchronous output spike volleys. Using a different way of measuring synchrony, the relation between input synchronization and output synchronization was also studied by Burkitt and Clark (2001).

Combining ideas from the preceding two paragraphs, a more accurate overall theory of PING may be created as follows. First, the approximate spike time distribution within the spike volleys of the E-cells, computed based on section 4, is taken into account in approximating the spike time distribution within the spike volleys of the I-cells. This yields a refinement of section 5, which in turn can be taken into account in approximating the spike time distribution within the spike volleys of the E-cells, leading to a refinement of section 4. Iterating this process, one may obtain increasingly accurate approximations to the spike time distributions within spike volleys. However, such an improved theory of PING is beyond the scope of this article.

While working on this project, we carried out far more simulations than have been presented here. Our conclusions hold over a wide range of pa-

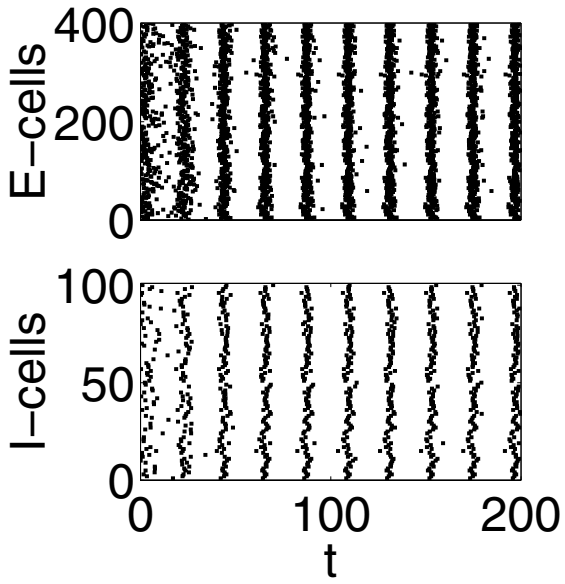

Figure 10: ING in an E-I network with sparse, random connectivity.

rameters. For instance, E→E synapses with $g_{EE} = 0.25$ have little effect on Figure 1B. Weak I→I synapses have little effect, except for the point made at the end of section 6.1: such synapses can make gamma rhythms possible in cases when the external drive to the I-cells is fairly strong. Strengthening I→I synapses often leads to a transition to a different synchronization mechanism, called ING by Whittington et al. (2000) and γ-I by Tiesinga et al. (2001). In ING, the I-cells are driven externally, not by the E-cells, and synchronize not only the E-cells but also themselves. For ING, the widths and shapes of the spike volleys of both E- and I-cells can be approximated using the ideas of section 4.1. Figure 10 shows a simulation with

$$g_{IE} = g_{II} = 0.25, \quad g_{EI} = g_{EE} = 0, \quad \tau_I = 10,$$
$$I_E = I_I = 0.1, \quad p_{IE} = p_{II} = 0.5.$$

As our theory would predict, the volleys of the E- and I-cells are now of equal duration. In future work, we will investigate ING in sparse, random networks in more detail, including in particular the effects of E → I-synapses.

Throughout this article, we have used the theta model. As remarked in section 2.1, the theta model is canonical for type I neuronal models in the sense that other type I models can be reduced to it by coordinate transformations (Ermentrout & Kopell, 1986; Hoppensteadt & Izhikevich, 1997). We therefore expect the picture to be qualitatively similar for all type I models,

even though the details of our calculations, and in particular the details of the centrally important Figure 5C, do depend on our choice of model. Whether and how our results generalize to type II models remains to be explored.

It would also be interesting to explore the effects of spike adaptation on our analysis. Synchronization in sparsely, randomly connected networks with spike adapation has been studied by van Vreeswijk and Hansel (2001). They discuss synchronization of bursts (not individual spikes) via adaptation (not inhibition) and observe that strong I $\rightarrow$ E synapses desynchronize bursts, in contrast with our regime, in which strong I $\rightarrow$ E synapses synchronize spikes. The model and analysis are so different from ours that a detailed comparison would be a major endeavor, but the article certainly suggests studying effects of adaptation in our model in the future.

We have analyzed synchronization by common input for the purpose of better understanding PING and ING. We remark, however, that synchronization by common input is also of neurobiological interest by itself (Usrey & Reid, 1999). We have shown that even very sparse input can synchronize and have analyzed the desynchronizing effect of heterogeneity in input strength.

Acknowledgments

We are grateful to Marcelo Camperi for stimulating discussions during the early stages of this work and to Steve Epstein for carefully reading the manuscript and providing helpful criticism. We thank the referees for interesting and useful comments. C. B. thanks the Center for BioDynamics at Boston University for a productive and pleasant visit during the spring of 2001, when this project was begun. His work was also supported by an equipment grant from Tufts University's Marshall Fund for Biomedical Research. N. K. received support from NSF grant DMS-9706694 and NIH grant MH47150.

References

Barkai, E., Kanter, I., & Sompolinsky, H. (1990). Properties of sparsely connected excitatory neural networks. *Phys. Rev. A, 41*, 590–597.

Braitenberg, V., & Schüz, A. (1998). *Cortex: Statistics and geometry of neuronal connectivity* (2nd ed.). New York: Springer-Verlag.

Brunel, N. (2000). Dynamics of sparsely connected networks of excitatory and inhibitory spiking neurons. *J. Comp. Neurosci., 8*, 183–208.

Brunel, N., & Hakim, V. (1999). Fast global oscillations in networks of integrate-and-fire neurons with low firing rates. *Neural Comp., 11*, 1621–1671.

Burkitt, A. N., & Clark, G. M. (2001). Synchronization of the neural response to noisy periodic synaptic input. *Neural Computation, 13*, 2639–2672.

Bush, P., & Sejnowski, T. (1996). Inhibition synchronizes sparsely connected cortical neurons within and between columns in realistic network models. *J. Comp. Neurosci., 3*, 91–110.

Diener, F. (1985a). Propriétés asymptotiques des fleuves. *C. R. Acad. Sci. Paris, 302*, 55–58.

Diener, M. (1985b). Détermination et existence des fleuves en dimension 2. *C. R. Acad. Sci. Paris, 301*, 899–902.

Diesmann, M., Gewaltig, M.-O., & Aertsen, A. (1999). Stable propagation of synchronous spiking in cortical neural networks. *Nature, 402*, 529–533.

Ermentrout, G. B. (1996). Type I membranes, phase resetting curves, and synchrony. *Neural Comp., 8*, 879–1001.

Ermentrout, G. B., & Kopell, N. (1986). Parabolic bursting in an excitable system coupled with a slow oscillation. *SIAM J. Appl. Math, 46*, 233–253.

Golomb, D., & Hansel, D. (2000). The number of synaptic inputs and the synchrony of large sparse neuronal networks. *Neural Comp., 12*, 1095–1139.

Gutkin, B. S., & Ermentrout, G. B. (1998). Dynamics of membrane excitability determine interspike interval variability: A link between spike generation mechanisms and cortical spike train statistics. *Neural Comp., 10*, 1047–1065.

Hansel, D., & Mato, G. (2001). Existence and stability of persistent states in large neuronal networks. *Phys. Rev. Lett., 86*, 4175–4178.

Hodgkin, A. L. (1948). The local changes associated with repetitive action in a non-medullated axon. *J. Physiol. (London), 107*, 165–181.

Hoppensteadt, F. C., & Izhikevich, E. M. (1997). *Weakly connected neural networks*. New York: Springer-Verlag.

Izhikevich, E. M. (1999). Class 1 neural excitability, conventional synapses, weakly connected networks, and mathematical foundations of pulse-coupled models. *IEEE Transactions on Neural Networks, 10*, 499–507.

Izhikevich, E. M. (2000). Neural excitability, spiking, and bursting. *Int. J. Bifurcation and Chaos, 10*, 1171–1266.

Mirollo, R. E., & Strogatz, S. H. (1990). Synchronization of pulse-coupled biological oscillators. *SIAM J. Appl. Math., 50*, 1645–1662.

Rinzel, J., & Ermentrout, G. B. (1998). Analysis of neural excitability and oscillations. In C. Koch & I. Segev (Eds.), *Methods in neuronal modeling* (pp. 251–292). Cambridge, MA: MIT Press.

Tiesinga, P. H. E., Fellous, J.-M., José, J. V., & Sejnowski, T. J. (2001). Computational model of carbachol-induced delta, theta, and gamma oscillations in the hippocampus. *Hippocampus, 11*, 251–274.

Tiesinga, P. H. E., Fellous, J.-M., José, J. V., & Sejnowski, T. J. (2002). Information transfer in entrained cortical neurons. *Network: Comput. Neural Syst., 13*, 41–66.

Tiesinga, P. H. E., & Sejnowski, T. J. (2001). Precision of pulse-coupled networks of integrate-and-fire neurons. *Network: Comput. Neural Syst., 12*, 215–233.

Traub, R. D., Jefferys, J. G. R., & Whittington, M. A. (1999). *Fast oscillations in cortical circuits*. Cambridge, MA: MIT Press.

Usrey, W. M., & Reid, R. C. (1999). Synchronous activity in the visual system. *Annual Review of Physiology, 61*, 435–456.

van Vreeswijk, C., & Hansel, D. (2001). Patterns of synchrony in neural networks with spike adaptation. *Neural Comp., 13*, 959–992.

van Vreeswijk, C. A., & Sompolinsky, H. (1996). Chaos in neuronal networks with balanced excitatory and inhibitory activity. *Science, 274*, 1724–1726.

van Vreeswijk, C. A., & Sompolinsky, H. (1998). Chaotic balanced state in a model of cortical circuits. *Neural Comp., 10*, 1321–1372.

Wang, X.-J., & Buzsáki, G. (1996). Gamma oscillation by synaptic inhibition in a hippocampal interneuronal network model. *J. Neurosci., 16*, 6402–6413.

Wang, X.-J., Golomb, D., & Rinzel, J. (1995). Emergent spindle oscillations and intermittent burst firing in a thalamic model: Specific neuronal mechanisms. *Proc. Natl. Acad. Sci. USA, 2*, 5577–5581.

Whittington, M. A., Traub, R. D., Kopell, N., Ermentrout, B., & Buhl, E. H. (2000). Inhibition-based rhythms: Experimental and mathematical observations on network dynamics. *Int. J. of Psychophysiol., 38*, 315–336.

Received February 11, 2002; accepted July 30, 2002.